Unveiling Water Ordering in Liquid-Liquid Phase Separation Using Bovine Serum Albumin-Polyethylene Glycol Systems

Giuseppe De Luca[1], Leonel Malacrida[2,3], Valeria Vetri[1]*, Giuseppe Sancataldo[1]

[1]Department of Physics and Chemistry – Emilio Segrè, University of Palermo, Viale delle Scienze, Ed.18, 90123, Palermo, Italy

[2]Advanced Bioimaging Unit, Institut Pasteur de Montevideo, Montevideo, Uruguay

[3]Facultad de Medicina, Unidad Académica de Fisiopatología, Hospital de Clinicas, Universidad de la República, Montevideo, Uruguay

*Corresponding author: valeria.vetri@unipa.it

Abstract

Liquid-liquid phase separation (LLPS) is a fundamental physicochemical process where a homogeneous liquid solution spontaneously separates into two distinct liquid phases. Initially studied in polymer science, LLPS has emerged as a crucial mechanism in various biological processes, particularly in the formation of membrane-less organelles within cells. These organelles are biomolecular condensates that compartmentalise biochemical reactions without relying on traditional lipid membranes. LLPS is driven by a balance of enthalpic and entropic contributions, with protein-protein and protein-solvent interactions playing a pivotal role. Environmental factors, including temperature, pH, and solute concentrations, critically influence these interactions and thus the phase separation process.

In this study, we investigate the role of water dynamics in the regulation of LLPS processes using a binary system of Bovine Serum Albumin (BSA) and Polyethylene Glycol (PEG). Classical spectroscopic methods and fluorescence lifetime imaging microscopy (FLIM), combined with phasor plot analysis, are employed to probe the local environment within protein condensates. Central to this approach is the use of 6-acetyl-2-dimethylaminonaphthalene (ACDAN), a fluorescent dye renowned for its sensitivity to water dipolar relaxation and changes in solvent polarity. This research aims to deepen our understanding of LLPS, particularly the role of water, offering insights into cellular processes and potential therapeutic strategies for LLPS-related diseases.

Keywords: Liquid-Liquid Phase Separation, Bovine Serum Albumin, Fluorescence Lifetime Imaging Microscopy, Water relaxation, Molecular Order, Spectroscopy

1. Introduction

Liquid-liquid phase separation (LLPS) is an intriguing physicochemical phenomenon that has garnered substantial attention in recent years across a broad spectrum of scientific disciplines[1–7]. This process entails the spontaneous separation of a homogeneous liquid solution into distinct liquid phases, each characterized by different compositions. Initially explored within the realm of polymer science, LLPS has emerged as a pivotal mechanism in a wide array of biological processes, including the formation of membrane-less

organelles within cells[8,9]. These organelles are coacervates constituted by dynamic, liquid-like biomolecular condensates that compartmentalize specific biochemical reactions, contributing to cellular organization and function without the need for traditional lipid membranes[10–12]. Although LLPS can happen in diverse solutions, processes involving proteins are of particular interest. LLPS is driven by a balance of enthalpic and entropic contributions[6–8,10]. Enthalpic contributions arise from favourable intermolecular interactions, such as hydrogen bonds, van der Waals forces, and electrostatic interactions, between the aggregated molecules. These interactions lower the overall enthalpy of the system, stabilizing a protein-dense phase. The entropic contribution to LLPS is more difficult to evaluate because the process creates two phases with markedly different entropic characteristics. In the dense phase, water molecules are more bound and restricted due to their interactions with the concentrated protein molecules, resulting in lower entropy with respect to the homogeneous phase[13]. Conversely, in the dilute phase, water molecules are less constrained and behave more like bulk water, contributing to higher entropy[14]. This significant difference in water molecule behaviour between the two phases complicates the accurate assessment of the overall entropic contribution to the phase separation process. Nevertheless, enthalpically favourable multivalent protein-protein interactions and protein-water interactions are necessary for LLPS to occur. In particular, the coacervation process takes place when protein-protein interactions become more favourable than protein-water interactions, resulting in the protein association. Importantly, the balance between these interactions can be influenced by the unavailability of water molecules to form hydrogen bonds with protein molecules, due to the structure and molecular order of water. These can be experimentally tuned by adding kosmotropic or chaotropic agents. Kosmotropic compounds stabilise the hydrogen bonding network of water, making it more ordered. This enhances the folding and stability of proteins by promoting stronger hydrophobic effect[15,16]. In contrast, chaotropic compounds disrupt the water's hydrogen bond network, increasing its disorder. This destabilises protein structures by weakening hydrophobic effect, often leading to protein unfolding or denaturation[17,18].

Notably, diverse factors such as environmental conditions (pH, temperature, presence of surfaces), concentration, and protein identity, influence whether the solution undergoes phase transition[12,19–22]. In this context, the contribution from hydration water to the LLPS is essential to study but nevertheless, it is largely unanalyzed[14,23]. Although involved in protein supramolecular assembly[24–27], the contributions of local hydration water to the thermodynamics of protein interactions are challenging to map accurately. Standard calorimetry approaches, which are typically used to study these interactions, cannot provide the detailed local mapping required to understand these contributions fully[28,29]. Additionally, the local hydration environment around proteins is influenced by numerous factors, making it a complex system to study. In a recent study by Pezzotti et al.[13] THz spectroscopy was used to explore the role of hydration water in LLPS, showing the entropic gain from realising bound-water during LLPS process undergone by α-elastin.

The driving molecular mechanisms underlying the formation of membrane-less organelles via LLPS are often studied in vitro using model systems to control and selectively manipulate the experimental condition. This allows for a detailed analysis of the fundamental principles governing phase separation, free from the complexities of the cellular milieu. By investigating this process in vitro, it was observed that, similarly to aggregation processes, LLPS is a general process which can occur for many, if not all proteins[7,19]. Both intrinsically disordered proteins and well-structured proteins were observed to undergo LLPS process, resulting in the formation of spherical liquid coacervates. Moreover Wang et al.[30] have more recently reported that even oligomeric peptides may undergo LLPS in vitro in specific experimental and solution conditions, further suggesting the universality of this process. In particular, this phase separation is favoured by factors such as low temperature, crowding agents like polyethylene glycol (PEG), and pH levels close to the isoelectric point. Depending on the solution conditions, coacervates may be composed by one molecular

species (homotypic coacervation) or by two or more molecular species (heterotypic coacervation). Coacervation occurs through protein self-association following variations in the environmental conditions such as temperature, pressure, pH, etc.[19,31–34]. LLPS is a reversible phenomenon that allows phase-separated droplets to dynamically form and dissolve in response to changes in the surrounding environment. In this context, protein association can be considered regulated by the same interactions which govern the aggregation process, but to a different extent, since the interactions within a liquid phase are weaker and possibly transient.

To gain deeper insights into the molecular forces driving LLPS, and to elucidate the role of biomolecular ordering and specifically the role of water in this process, we designed an experimental study using a binary system composed of Bovine Serum Albumin (BSA) and Polyethylene Glycol (PEG) in an aqueous acetate buffer close to the isoelectric point of BSA (about pH 4.6)[35,36]. BSA, a globular protein known for its well-established water solubility and relevance as a model system, provides a suitable platform for probing LLPS[19,37–40]. It has a well-characterised structure and properties, high stability and high purity and availability[41,42] make it an ideal candidate for studying the interplay of protein interactions and phase separation in aqueous environments. PEG, a versatile synthetic polymer commonly used in biomedical and pharmaceutical applications, introduces an additional layer of complexity to the phase behaviour of the system. Systems containing BSA and PEG in various experimental conditions were already studied showing the formation[19] and the ageing of BSA coacervates[40] and the feasibility of the compartmentalization of enzymatic reactions in protein-rich droplets[39]. The presented experiments are designed to elicit the role of water and its ordering in LLPS processes, offering a window into the molecular dynamics that drive the formation of coacervates and other phase-separated structures. By using chaotropic and kosmotropic compounds such as Ethanol (EtOH) and Glycerol, we were able to modulate the ordering of water in the system and to analyse its effect on the LLPS process. To explore the molecular ordering changes during LLPS, we employ a combination of spectral and microscopy techniques to investigate the governing forces behind LLPS. Spectral analysis and fluorescence lifetime imaging microscopy (FLIM) are integrated with phasor plot analysis to probe the local nano-environment within protein condensates. ACDAN (6-acetyl-2-dimethylaminonaphthalene) is a fluorescent dye with unique photophysics to study water dipolar relaxation on its near environment[43–46]. ACDAN respond to dynamics changes in water dynamics and environmental dielectric properties (such as polarity), render it an invaluable tool for investigating the microenvironment within phase-separated systems. By analysing the fluorescence behaviour of ACDAN in our BSA-PEG system, we can characterise changes in water dynamics within protein condensates under varying experimental conditions. This approach allows us to provide quantitative evaluation of the physicochemical microenvironment of condensates. ACDAN, widely utilised in water studies and analytical chemistry, exhibits fluorescence characteristics that make it particularly useful for investigating water state, dynamics, and interactions at a molecular level. When introduced into bulk water, ACDAN undergoes to spectral shifts in response to water dipolar relaxation around it. This property is a powerful proxy of the micro-environmental conditions. This property extends its applicability to a range of studies, including the probing of hydration dynamics in biomolecules and the exploration of water organisation in different phases. By exploiting ACDAN's unique properties in our study, we aim to deepen our understanding of LLPS, particularly the critical role that water plays in the formation and stability of biomolecular condensates. Our results clearly demonstrate that molecular order of water plays a crucial role in governing the LLPS process. Furthermore, we observed that the two resulting phases exhibit distinctly different microenvironmental characteristics: the diluted phase presents a higher polarity and a higher dipolar relaxation while the concentrated phase presents a lower polarity and a lower dipolar relaxation. These observations indicate that biomolecular order drives the separation and determines the local properties and molecular dynamics within each phase. These findings show an intrinsic link between

molecular architecture and the microstructure of the separated phases, opening new perspectives for understanding the mechanisms underlying LLPS and their biological implications.

2. Materials and Methods

Sample preparation: Stock solutions of 50 mg/ml (0.75 mM) BSA and 500 mg/ml (125 mM) PEG 4000 (purchased by Sigma-Aldrich) were prepared in 100 mM acetate buffer (pH 4.6). Upon 1:10 dilution of the BSA stock, BSA concentration was measured by UV – Vis spectroscopy by means of a Jasco – V770 spectrophotometer using the molar extinction coefficient ε = 0.667 ml cm^{-1} mg^{-1} at 280 nm. The sample is prepared by mixing BSA and PEG at room temperature to the desired concentration: 25 mg/ml (0.38 mM) BSA and PEG concentration between 60 mg/ml (15 mM) and 76 mg/ml (19 mM). The sample is always prepared adding the buffer, PEG 4000 and BSA in this order. Before adding BSA to the mixture, PEG and buffer are mixed until the solution is homogeneous. For the experiments involving the non-polar chaotropic and kosmotropic agents, 50% (v/v) (6.8 M) glycerol and 20% (v/v) (3.4 M) EtOH stock solution were prepared in the same acetate buffer and then added to the sample at the desired concentration (EtOH final concentration ranges between 1% - 4% (v/v) (17 mM – 68 mM) and glycerol final concentration ranges between 2% - 8% (v/v) (27 mM – 1.1 M)). For ACDAN experiments in bulk, ACDAN is added to a final concentration of 30 µm. To characterise the two aqueous phases, formed following an LLPS process, the solution was physically separated by centrifugation (10^4g for 10 min at 20°C) of a sample containing 25 mg/ml (0.38 mM) BSA, 76 mg/ml (19 mM) PEG 4000, 30 µm ACDAN in 100 mM acetate buffer (pH 4.6). The homogeneous phase consists of a sample containing 25 mg/ml BSA, 68 (17 mM) mg/ml PEG 4000, and 30 µm ACDAN in 100 mM acetate buffer (pH 4.6).

Scattering measurements: Scattering measurements were acquired using a Jasco-FP-8500 spectrofluorometer equipped with a Jasco ETC-815 Peltier cell as temperature controller. Rayleigh scattering at 90° was registered as the maximum of the elastic peak of excitation light at 650 nm. A 1 cm pathlength quartz cuvette has been used. The response time was set to 1 s, data interval to 0.1 nm, scan speed to 100 nm/min, and excitation and emission bandwidths to 2.5 nm. Spectra were acquired at each degree Celsius during a temperature ramp of -15°C/hour (from 35°C to 0°C).

Fluorescence measurements: Fluorescence spectra in bulk were acquired using a Jasco-FP-8500 spectrofluorometer equipped with a Jasco ETC-815 Peltier cell as a temperature controller. ACDAN fluorescence spectra were acquired in 1 cm path-length quartz cuvettes. The response time was set to 1 s, data interval to 0.5 nm, scan speed to 100 nm/min, and excitation and emission bandwidths to 2.5 nm. The acquisition range is 380 nm – 650 nm and the excitation wavelength is 390 nm. Spectra were acquired at each degree Celsius during a temperature ramp of -15°C/hour.

Generalized Polarization of Fluorescence measurements:

ACDAN fluorescence spectra were analysed in terms of Generalised Polarization function (GP) that was calculated using the following formula adapted from Parasassi et al.[47].

$$GP = \frac{I_{450} - I_{560}}{I_{450} + I_{560}}$$

where I_{450} and I_{560} are the fluorescence intensity at the corresponding wavelengths. The increase of the GP values indicates a spectral blueshift of the fluorescence band, while its decrease indicates a spectral redshift.

Spectral Phasor analysis of Fluorescence measurements:

The spectral phasor analysis is a geometrical representation of the fluorescence spectra obtained by transforming them into a point (phasor) in a polar plot, called a spectral phasor plot. The x-coordinates (g) and the y-coordinates (s) are obtained as the real and imaginary part of the first harmonic of the Fourier transform of the spectra. Fluorescence spectra are therefore mapped within a circle centred at the origin of the axes (0; 0) and radius 1. In the spectral phasor plot, the angular position (phase) is measured from the positive x-axis in the counterclockwise direction, and the modulation is measured radially from the origin to the circumference. The angular position is related to the centroid of the fluorescence spectra: spectra centred at shorter wavelengths have a low angular position, while spectra centred at longer wavelengths have a higher angular position. The modulation is related to the FWHM (full width at the half maximum) of the band: at increasing modulation, the corresponding spectrum is less broad. A detailed description of this method is reported in the works by Fereidouni et al.[48,49] and Malacrida et al.[50,51].

Two-photon microscopy: The experiments were performed using a Leica TCS SP5 confocal laser scanning microscope, with a 63×/1.40-0.60 oil objective, and a scanning frequency of 400 Hz (Leica Microsystems, Germany). ACDAN fluorescence was excited at 780 nm (Spectra-Physics Mai-Tai Ti:Sa ultra-fast laser). All the images were acquired at a resolution of 1024 × 1024 pixels and the detection range was 450 – 600 nm. The fluorescence spectra were obtained by acquiring 256 × 256 pixels images with a 15 nm bandwidth and 5 nm step size in the detection range was 400 – 650 nm. The analysis of the microscopy data was performed by the open-source software ImageJ Fiji (https://imagej.net/software/fiji/).

Fluorescence Lifetime Imaging Microscopy (FLIM): FLIM measurements were acquired in the time domain by means of a Leica TCS SP5 confocal laser scanning microscope coupled with picoHarp 300 TCSPC module (Picoquant, Germany). 256 × 256 pixels FLIM images were collected with a 63×/1.4 oil objective and a scanning frequency of 400 Hz. ACDAN fluorescence was excited at 780 nm (Spectra-Physics Mai-Tai Ti:Sa) and it was collected in two channels: 430 – 460 nm (blue channel) and 550 – 580 nm (green channel).

Phasor approach analysis of FLIM data:

FLIM data were analysed by means of the phasor approach, introduced by Digman and colleagues in 2008[52]. The phasor approach allows for a graphical representation of FLIM data, by mapping the fluorescence exponential decays collected at each pixel of a FLIM image into phasors on a polar plot, known as phasor plot, through the Fourier transform. The x-axis and the y-axis of the phasor plot are the real (g) and imaginary (s) parts of the Fourier transform of the fluorescence decays. All the fluorescence decays are mapped on a semicircle, known as universal circle. It is centred at the point of coordinates (0.5; 0) and has a radius of 0.5. The universal circle extends from the point (1; 0), where shorter lifetime ($\tau = 0$) are mapped to the point (0; 0) where longer and virtually infinite lifetime ($\tau = \infty$) are mapped. Single-exponential (single-component) decays lie on the universal circle, and multi-exponential (multi-component) decays lie within it. FLIM data analysed by means of the phasor approach are displayed in the phasor plot as clouds of points for each measured fluorescence lifetime, thus called the lifetime distribution. The lifetime distribution can be selected by coloured cursor which marks the pixel associated with the selected distribution by the same colour. This feature allows to spatially localize the fluorescence lifetime of the original image and results in the formation of a phasor map, a new image, coloured in false colours that provide information on the spatial distribution of the fluorescence lifetimes[53].

FLIM analysis was performed by the SimFCS4 software developed at the Laboratory of Fluorescence Dynamics, University of California at Irvine (http://www.lfd.uci.edu). The fluorescence lifetime of Alexa 405

(τ = 3.6 ns, single exponential[54]) was used to calibrate FLIM data in the blue channel. The fluorescence lifetime of fluorescein (τ = 4 ns, single exponential[55]) was used to calibrate FLIM data in the green channel.

3. Results and discussion

3.1 Liquid-liquid phase separation induced by thermal treatment

The dynamic process during LLPS of BSA-PEG solution was investigated, by using temperature as a triggering physical parameter for phase transition. The solution consists of 25 mg/ml BSA dissolved in 100 mM Acetate buffer at pH 4.6 in the presence of PEG-4000, as molecular crowding agent. Figure 1 a) shows a schematic representation of the investigated system: the left side of the figure depicts the solution at high temperatures (35°C), where it appears homogeneous and clear. The right side illustrates the phase separation that occurs upon cooling, leading to the formation of small liquid coacervates, shown as light green circles. As a result, from a macroscopic point of view, the solution becomes turbid and whitish. In Figure 1b) a representative transmission image acquired of the sample following the LLPS is shown. Specifically, this sample contains 76 mg/ml PEG-4000, and the BSA coacervates appear as spherical drops which float in the solution. Diameters of the droplets range from a few micrometres to 20 micrometres.

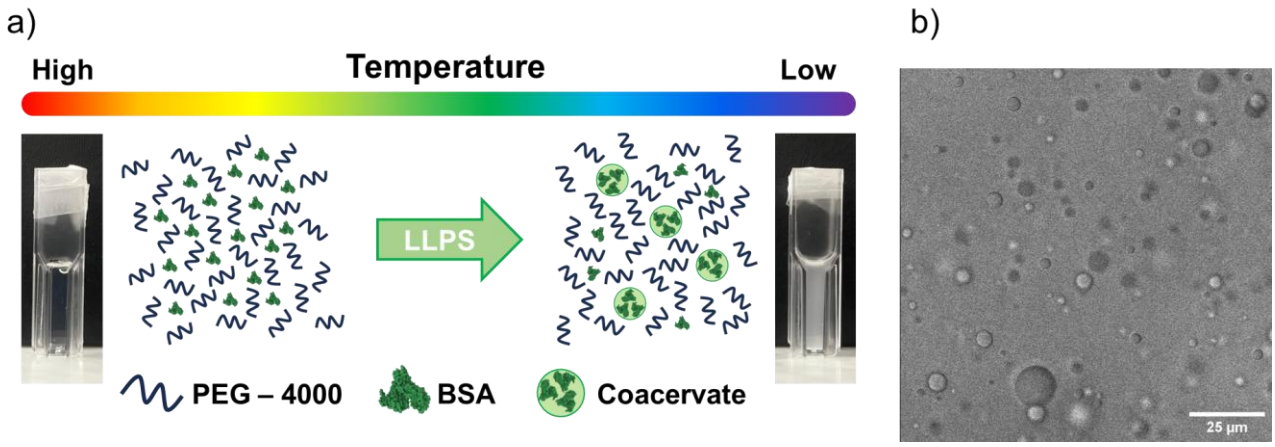

Figure 1. *a) Schematic representation of the investigated system, that consists in an aqueous solution of 25 mg/ml BSA and PEG-4000 as crowder agent in 100 mM acetate buffer at pH 4.6. At higher temperatures (35°C) the sample is a homogeneous solution and appears transparent. By lowering the temperature, it undergoes a phase separation resulting in the increase of turbidity due to the formation of coacervates. b) 1024×1024 pixels representative optical microscopy image of the solution containing 76 mg/ml PEG-4000 at room temperature (23°C).*

To investigate the effects of PEG concentration on BSA-PEG LLPS, we monitored the scattering intensity of the solution throughout the transition in samples with varying PEG content. during the temperature ramp from 35°C to 0°C (scan rate is -15°C/hour). The elastic scattering was measured at 650 nm i.e. where no absorption or fluorescence signal is expected from the sample. In Figure 2a) the scattering intensity as a function of temperature is reported for samples containing PEG at concentrations, ranging from 60 mg/ml to 76 mg/ml. During a decreasing temperature ramp, all samples exhibited an increase in scattering intensity below a certain transition temperature. At temperatures lower than this threshold, a relatively linear growth in signal intensity is observed until reaching a certain point, after which the intensity begins to decrease due to sample sedimentation (data not reported). Specifically, when the solution is in a single phase, it remains homogeneous and transparent, leading to negligible scattering intensity. When cooled below the transition temperature, the solution begins to separate into two phases. At the macroscopic level, the phase separation

is evident as the sample solution becomes turbid. Interestingly, the LLPS process can be reversed, bringing back the sample to 35°C and agitating it to mix the two phases.

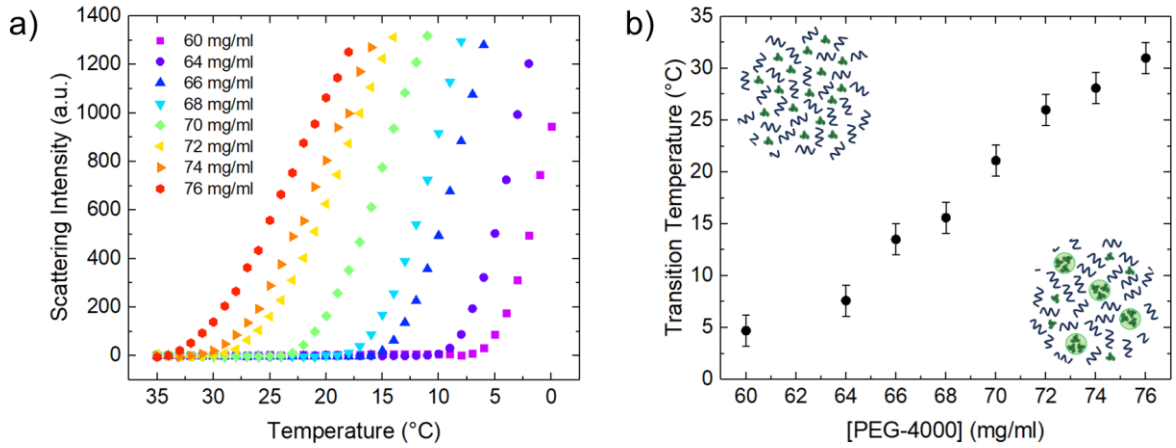

Figure 2 *a) Scattering intensity of 25 mg/ml BSA, PEG-4000 solution in 100 mM acetate buffer at pH 4.6 measured at 650 nm as a function of temperature. The scan temperature rate is -15°C/hour. When the solution is homogeneous the scattering intensity at this wavelength is negligible, but it dramatically increases when the sample undergoes a phase separation. With increasing PEG concentration, the LLPS in the sample occur at increasing temperatures. Transition temperature can be defined as the x-intercept of a linear fit of the scattering intensity during the growth phase. b) Transition temperatures as a function of PEG concentrations. The transition temperature increases with increasing PEG concentration.*

As it is evident, at higher PEG concentrations, the onset of increased scattering intensity occurs at higher temperatures. To highlight this effect the scattering intensity measurements in the growth region were fitted using a straight line, and the transition temperature was determined as the resulting x-intercept at each PEG concentration (see Figure S1 as an example). These data are reported in Figure 2b), representing a branch of the phase diagram of the sample. Above the experimental points, the solution is homogeneous, while below these points, the solution separates. These observations are in line with previous published results[34,56,57] and can be rationalised considering that the excluded volume effect which induces LLPS, depends on the concentration of the crowding agent in solution[58,59].

In the investigated system, LLPS is primarily driven by molecular crowding. As a molecular crowder, PEG induces excluded volume effects and therefore depletion forces between BSA molecules[60–63], which act as attractive protein-protein interactions. Consequently, these forces favour the phase transition by promoting the association of BSA molecules. At high temperatures, the repulsive forces are dominant resulting in a homogeneous phase, while at low temperatures, the depletion forces between BSA molecules overcome the repulsive interactions which govern the homogeneous phase. Therefore, by lowering the temperature, the balance among the various forces acting in solution is shifted. The “transition temperature” thus corresponds to the temperature at which this balance is inverted, and the attractive depletion forces become dominant over repulsive interactions. Thus, below the transition temperature LLPS occurs[39,64–67].

Notably, by working at the BSA isoelectric point, we were able to rule out the electrostatic effects arising from its charge, therefore simplifying the overall picture and artificially enhancing the contribution of the depletion interactions. The presence of PEG may impact LLPS involving a complex interplay of various effects, such as excluded volume, changes in solution viscosity, modification of dominant short- and long-range interactions and water ordering. In this case, the fact that the temperature transition depends quite linearly on the PEG concentration is an indication that, in the analysed concentration range, LLPS is induced mainly by the exclusion volume effects, and not by other specific interactions (e.g., between PEG and BSA) which could arise within the solution[57]. This effect is further suggested by the fact that the scattering data at

different PEG concentrations present a linear region with similar slopes, indicating that the same LLPS process occurs in each sample and that the PEG concentration does not affect the propensity of BSA to undergo LLPS.

3.2 Phase stability alteration induced by non-polar kosmotropic and chaotropic agents

The presence of PEG may modify hydration level, possibly impacting protein stability and giving rise to the entropically driven formation of protein assemblies[68–70]. To investigate the role of water and molecular ordering in the LLPS process, we analyse how chaotropic and kosmotropic compounds influence water ordering and the LLPS behaviour under examination. In particular, non-ionic disordering and ordering compounds were selected: EtOH was used as a chaotropic agent[71] and Glycerol as a kosmotropic one[72]. Performing analogous studies either at pH far from the isoelectric point or using salt of the Hofmeister series[20,73], which induce significant modification in water structure, can lead to the occurrence of strong intermolecular electrostatic interactions. These long-range interactions may overshadow the contribution of weaker potential or transient interactions, such as Van der Waals forces or hydrogen bonding, which are mediated by water molecules, effectively masking the role of water in this context. The choice of using these non-ionic compounds, in conditions where BSA is globally neutral, allows us to reduce and to negligible such long-range electrostatic interaction effects.

In Figure 3 the analysis of the LLPS behaviour of a 25 mg/ml BSA, 68 mg/ml PEG-4000, in 100 mM acetate buffer at pH 4.6 in the presence of EtOH and Glycerol at different concentrations is reported. Analogous experiments to the ones in Figure 2 were performed. These experiments are aimed at evaluating whether and how different concentrations of these additives impacted LLPS. PEG concentration was selected to optimise measurement conditions allowing to have similar dynamical range both above and below the transition temperature. From now on the 25 mg/ml BSA, 68 mg/ml PEG-4000, in 100 mM acetate buffer at pH 4.6 sample will be referred to as the standard sample.

Figure 3a) shows the scattering intensity as a function of the temperature (from 35°C to 0°C) at various concentrations of EtOH. As evident, in the temperature range explored here, the scattering data acquired in the presence of EtOH have analogous profiles to the ones acquired in the absence of EtOH. At increasing EtOH concentrations, scattering data are shifted towards higher temperatures. At concentrations higher than 4% (v/v), the sample undergoes LLPS at temperatures above 35°C. In Figure 3b) the transition temperatures for each temperature scan are reported revealing also in this case a quite linear behaviour. All of these data suggest that EtOH affects the LLPS occurrence in a concentration-dependent manner, but it appears to not affect the molecular mechanisms at the basis of LLPS. EtOH is known to induce modifications in the hydration shell of protein molecules[74–79]. This significantly destabilises the protein conformational state, leading to a loss of its three-dimensional structure, and a looser structure[80]. This, in turn, modifies protein-protein and protein-water intermolecular interactions, and it was described for many proteins, including BSA[81–84]. In particular, larger surface area enables a greater number of protein-protein interactions, that therefore facilitate LLPS. This effect is known to be concentration-dependent, in line with the presented results[74,79,81,85]. However, it should be noted that direct interaction between EtOH and BSA cannot be unequivocally excluded.

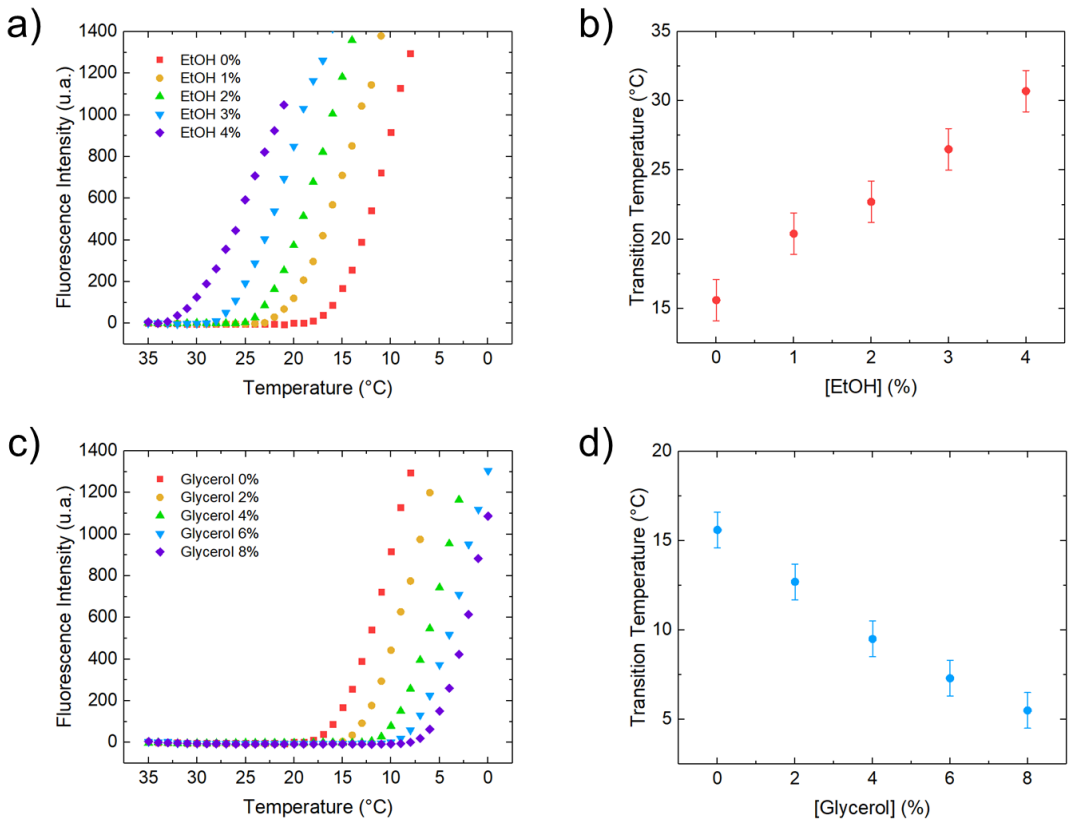

Figure 3 *Effect of non-ionic chaotropic and kosmotropic agents on LLPS process. a) Scattering data of the standard sample (25 mg/ml BSA, 68 mg/ml PEG-4000, in 100 mM acetate buffer at pH 4.6) during a temperature ramp from 35°C to 0°C (scan rate = -15°C/hour) with different concentrations (v/v) of EtOH as chaotropic agent. Increasing the ethanol concentration, the LLPS occurs at higher temperatures. b) Transition temperature measured as described before increases linearly with the ethanol concentration. c) Scattering data of the standard sample during the same temperature ramp of the previous experiments with different concentrations (v/v) of glycerol as kosmotropic agent. LLPS occur at lower temperatures as the glycerol concentration increases, denoting that glycerol stabilises the sample. d) Transition temperature decreases with the EtOH concentration.*

Figure 3c) shows the effect of Glycerol on the LLPS undergone by BSA. Similarly to what was reported above, scattering measurements are reported as a function of temperature on the standard sample at increasing Glycerol concentrations. Interestingly, these data present analogous profiles to the ones in Figure 2a) and Figure 3a), supporting the idea that a common denominator exists regulating the observed LLPS. Opposite to EtOH, at increasing Glycerol concentration scattering data are shifted towards lower temperatures. This indicates that the addition of Glycerol to the sample makes the LLPS process less energetically favourable, eventually inhibiting LLPS at concentrations above 8% (v/v) in the analysed temperature range. In Figure 3d), the transition temperatures obtained from each temperature scan, as described above, are reported, revealing also in this case a quite linear trend. Similarly to EtOH, Glycerol influences the LLPS in a concentration-dependent manner, mainly affecting only the transition temperature of the process.

It should be noted that Glycerol is a very soluble compound that forms strong hydrogen bonds with water molecules, acting as a kosmotropic agent[86]. Being strongly hydrophilic, glycerol molecules bind strongly to 2 to 4 water molecules, with an average of 5.58 water molecules in its hydration shell[87]. As a result of increased stability of protein structure[85,88], the intermolecular protein interactions are disfavoured, and therefore LLPS and more in general the supramolecular assembly process are reduced. Notably, the change in the LLPS and in the transition temperatures cannot be ascribed to changes in viscosity. At room temperature, the viscosity of water is about 1 mPas and the viscosity of 10% glycerol is about 1.3 mPas[89], while the viscosity of a slightly

smaller PEG (3350 Da) at a similar concentration is about 6.1 mPas[90]. These values denote that the glycerol contribution to the viscosity of the solution is negligible with respect to the PEG contribution.

The observation that Glycerol presence reduces the transition temperature supports the idea that water molecule order affects standard sample LLPS. Indeed, Glycerol molecules are thermodynamically favoured to be preferentially excluded from the hydration shell of protein molecules[91] and its presence of Glycerol produces a more ordered and stable hydration shell of protein molecules.

3.3 Water structure order using ACDAN fluorescence

Data presented in the previous section support the idea that excluded volume effects induced by PEG in solution favour phase transition. These effects are modulated by chaotropic and kosmotropic compounds, which modify water ordering, affecting protein stability and their tendency to form coacervates. This leads to the question of how and if the molecular order of the system changes during the phase transition. To gain useful insights we exploit the spectroscopic properties of ACDAN (6-acetyl-2-dimethylamino naphthalene). This molecule is a fluorescent probe from the DAN family and among LAURDAN and PRODAN it is the most hydrophilic[43,44].

To the best of our knowledge, being highly soluble, ACDAN is used in literature to investigate the dipolar relaxation of water in crowded milieus both in vitro and in vivo[44–46,92–94], connecting it to the rotational dynamics of water. For instance, Ambroggio et al.[94] observed the LLPS of the capsid proteins of the Dengue virus and the Zika virus and reported how the water relaxation sensed by ACDAN within the coacervates of these two proteins were different and how their structure may therefore impact on the structure of water. Thoke et al.[93], reported how ACDAN fluorescence can probe in vitro the water dynamics in yeast cells (Saccharomyces cerevisiae) during the metabolism of glucose, detecting a strong coupling between ACDAN fluorescence intensity and the concentration of both ATP and NADH. They moreover highlighted how ACDAN does not partition in cellular membranes, being highly hydrophilic. Vorontsova et al.[45] used ACDAN as a tool to quantitatively monitor the water activity to study in vivo the macromolecular crowding in a zebrafish ocular lens.

ACDAN fluorescence depends on both the dipolar relaxation and the polarity of the solution[43,44,93,95,96]. The dipolar relaxation is the ability of the dipoles in solution to rotate and to be re-oriented by ACDAN dipole moment in the excited state. Higher dipolar relaxation indicates less constrained water molecules and thus a more disordered state, while lower dipolar relaxation indicates hindered rotation of the molecules, related to a more rigid and ordered state[44,96,97]. Recently, we were able to elucidate the correlation between the spectral changes of ACDAN fluorescence and the water ordering using simple model systems[96]. A schematic Jablonsky diagram of ACDAN is shown in Figure 4a). Following the absorption of a photon, ACDAN is in an excited state. At this state the solvent molecules can reorient or relax around the dipole moment of the ACDAN molecules, which lowers the energy of its excited state, depending on the degree of the solvent dipolar relaxation (referred as DR in Figure). This results in a spectral shift of the fluorescence band: when ACDAN experiences a higher dipolar relaxation of the solution (disordered water), its fluorescence spectrum is red-shifted, while if the dipolar relaxation is lower (ordered water), ACDAN fluorescence is blue-shifted. As a consequence of ACDAN's sensitivity to dipolar relaxation, it is also responsive to the polarity of its surroundings. In fact, a more polar environment consists of molecules with a higher dipole moment, which are more likely to relax around the dipole of ACDAN. Conversely, in a less polar environment, composed of molecules with a low or absent dipole moment, ACDAN is nearly unaffected, resulting in only a small portion

of its excited state energy being dissipated. Thus, when the dye is in a polar solvent, the fluorescence red-shifts; otherwise, it blue-shifts. Therefore, changes in the fluorescence spectrum of ACDAN may be attributed to both of these effects, which are related yet have distinct physicochemical implications that are difficult to disentangle.

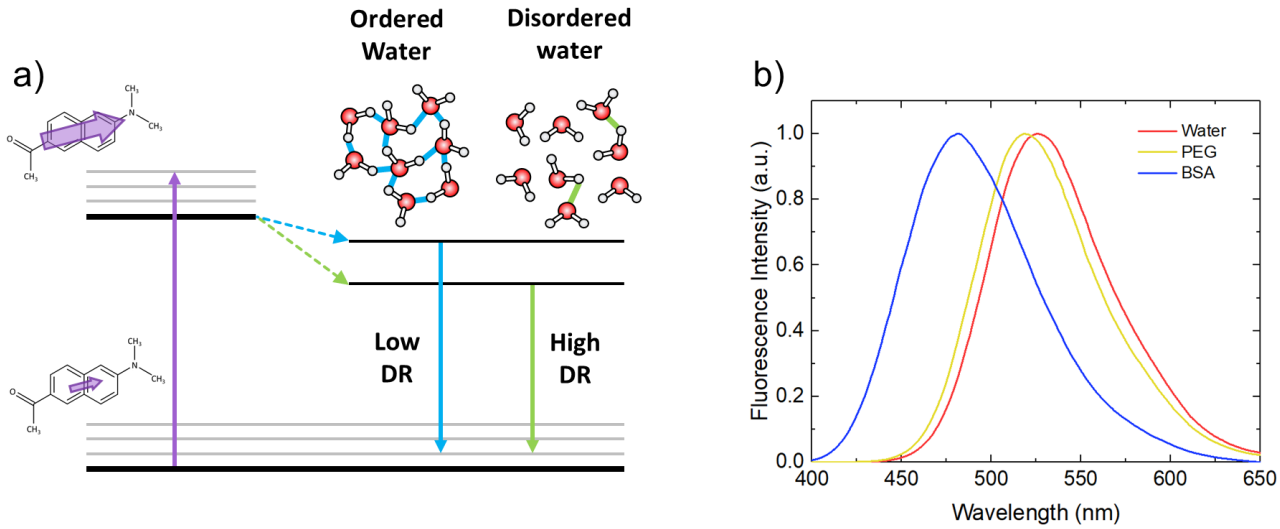

Figure 4 *a) Simplified Jablonski diagram for ACDAN dye: the absorption transition between the ground state and the excited state is shown by a purple arrow. In the excited state, ACDAN has a higher dipole moment. ACDAN molecules couple with solvent molecules and reorganise them. This results in the lowering of the energy of the excited state, depending on the degree of solvent dipolar relaxation (referred as DR in the Figure). When the dipolar relaxation is high (disordered water) the level is less energetic and the fluorescence of ACDAN is red-shifted, while when the dipolar relaxation is low (ordered water) the fluorescence is blue-shifted. b) Normalised fluorescence spectra of 30 µM ACDAN in water (red), in presence of 25 mg/ml BSA (blue), and in presence of 68 mg/ml PEG (yellow) at 23°C. λ_{exc} = 390 nm, Excitation bandwidth = 2.5 nm, Emission bandwidth = 2.5 nm, scan speed = 100 nm/min, acquisition range = 390 nm - 650 nm.*

Figure 4b) shows the ACDAN fluorescence spectra in water (red spectrum), in the PEG sample (yellow spectrum) and in the BSA (blue spectrum) at 23°C. The PEG sample and the BSA sample consist respectively in 68 mg/ml PEG and 25 mg/ml BSA dissolved in 100 mM acetate buffer at pH 4.6. The spectrum of ACDAN in water is centred around 525 nm, while the spectrum measured in the PEG sample is blue-shifted by about 10 nm. This blue-shift is in line with an increase of molecular crowding due to the presence of PEG, in agreement with what has already been reported in literature[93]. However, in the presence of BSA, the ACDAN fluorescence spectrum undergoes a profound blue-shift of about 45 nm. This cannot be explained by the molecular crowding induced by BSA, also because the molar BSA concentration (about 0.38 mM) is several orders of magnitude lower than the one of PEG (about 17 mM), suggesting therefore an interaction between BSA and ACDAN molecules.

BSA is a transport protein renowned for its binding capabilities, attributed to its hydrophobic pockets[98–104]. These pockets enable BSA to interact with a wide variety of molecules also due to a structural flexibility of these binding sites. Moreover, PRODAN is known to interact with BSA, resulting in a spectral blue-shift and in an increase of fluorescence intensity, similar to what is observed here[43]. PRODAN and ACDAN are two similar molecules only differing by the presence of an ethyl group (PRODAN) instead of a methyl group (ACDAN), making PRODAN slightly more hydrophobic and therefore increasing its binding ability to hydrophobic pockets of BSA. ACDAN is sensitive to water dipolar relaxation, but it is not possible to exclude that the signal reflects the properties of hydration water protein. The spectral blue-shift indicates that either ACDAN experiences a more hydrophobic environment or a lower dipolar relaxation or both. Therefore, it is reasonable to speculate that some ACDAN molecules enter within the BSA pockets, sensing its hydrophobic

environment. This results in a spectral blue-shift due to the restricted mobility of the molecules within the pockets. This hypothesis was tested by acquiring the fluorescence spectra of ACDAN at increasing concentrations maintaining the BSA concentration constant. Results are shown in Figure S2, which demonstrates that as the ACDAN-BSA ratio increases, the fluorescence spectrum of ACDAN becomes narrower (as highlighted by the FWHM). This suggests that at low concentrations, ACDAN enters the BSA binding pocket, and as the concentration of ACDAN increases, the BSA pocket saturates, leading to an increased contribution from ACDAN in solution.

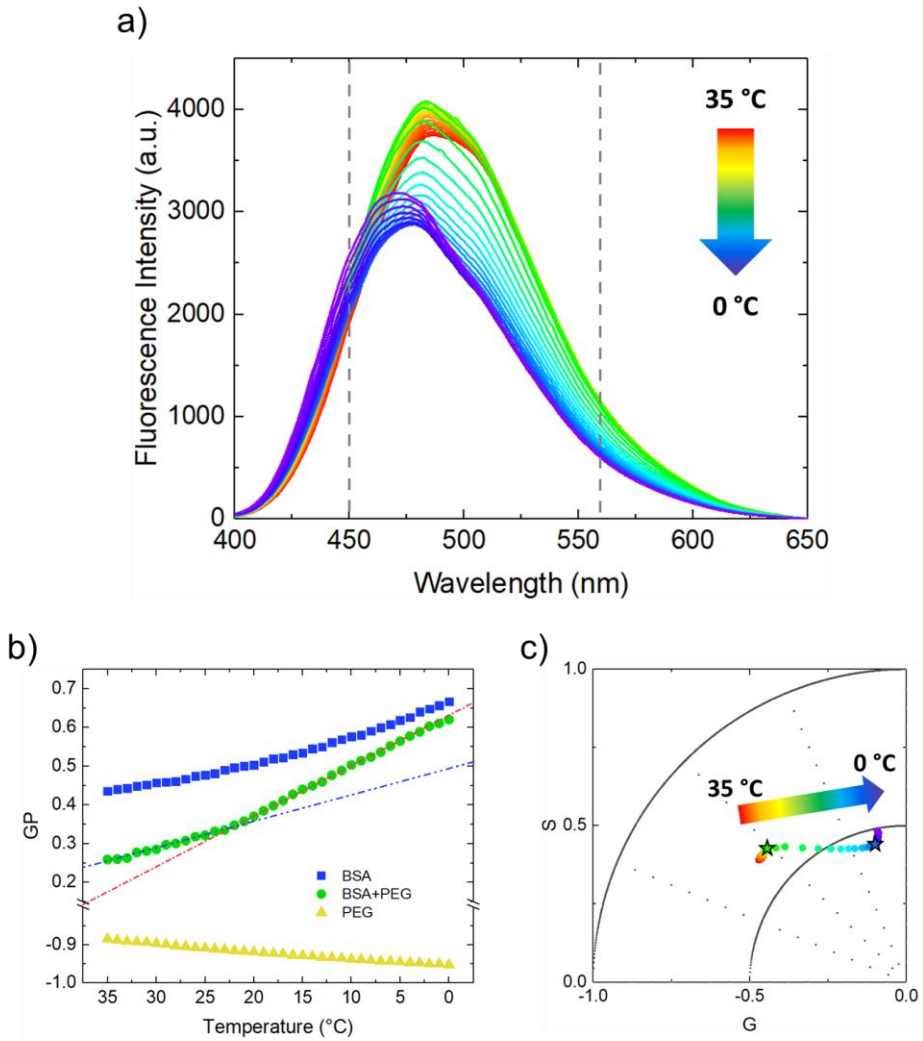

Figure 5 *a) Fluorescence kinetics of standard sample with the addition of ACDAN 30 µM during a temperature ramp from 35°C to 0°C (scan rate = -15°C/h), λ_{exc} = 390 nm, Excitation bandwidth = 2.5 nm, Emission bandwidth = 2.5 nm, scan speed = 100 nm/min, acquisition range = 390 nm - 650 nm). The fluorescence of ACDAN shows an overall blue-shift indicating the ordering of the system. The grey dashed lines are drawn at 450 nm and 560 nm, which are the chosen wavelengths for calculating the Generalised Polarisation function (GP). b) GP of ACDAN fluorescence spectra for the standard sample (BSA+PEG in green circles), a sample containing 25 mg/ml BSA (blue squares), and a sample containing 68 mg/ml PEG (yellow triangles) in the same 100 mM acetate buffer at pH = 4.6. GP of the standard sample shows a binodal trend, highlighted by the dashed lines. c) Spectral phasor analysis of the fluorescence spectra for the standard sample. The coloured arrows mark the sequence of points as the temperature decreases in the polar plot. The green and blue stars mark the data acquired at 21°C and 8°C respectively.*

Furthermore, we analysed the modification in the steady state fluorescence spectrum of ACDAN in the standard sample solution during the descended temperature ramp in the experimental conditions at which LLPS occurs. Figure 5a) shows the fluorescence spectra of ACDAN dye in the standard sample during a temperature ramp from 35°C to 0°C (the scan rate is 15°C/h). As can be seen, significant modifications occur

both in intensity, shape and position of the observed signal. The first spectrum measured at 35°C is centred at about 490 nm. By lowering the temperature, the overall fluorescence intensity increases and the spectral shape changes, towards shorter wavelengths. At about 21°C the fluorescence intensity starts to decrease, while continuing to blue-shift, until about 8°C. At this temperature, until the end of the temperature ramp, the fluorescence intensity increases again. Changes in fluorescence spectra clearly indicate a non-monotonic decrease of dipolar relaxation during the temperature scan. The observed spectral changes certainly result from the combined effects of modifications in the molecular environment experienced by ACDAN and the intrinsic effects of temperature. Indeed, at lower temperatures, the rate of the radiative pathway is higher. Moreover, at low temperatures the solvents usually become more viscous, and the time for solvent reorientation increases, resulting in the lowering of dipolar relaxation[105]. This would result in the increase in fluorescence intensity and in a blue-shift. It is reasonable to speculate that in the temperature range between 35°C and 21°C the spectra modifications are dominated by the thermal effects since macroscopic effects of LLPS are not observed (as shown in Figure 2a), cyan triangles). Conversely, in the range between 21°C and 8°C the fluorescence modifications are strongly affected by LLPS as the fluorescence intensity is observed to decrease. Similarly, below 8°C the fluorescence intensity starts to increase suggesting that modifications due to phase transition are completed. ACDAN fluorescence spectra during the temperature scan of control samples containing only PEG and BSA are reported in Figure S3, which show a monotonic increase of the fluorescence.

By comparing the ACDAN fluorescence spectra acquired in the PEG, BSA and standard sample at the same temperature, it is possible to notice that the latter present spectral features of ACDAN fluorescence acquired in the BSA and PEG sample. To show this aspect, in Figure S4 we reported the ACDAN fluorescence spectra in these three samples at two temperatures, 35°C (panel a) and 0°C (panel b).

Interestingly, at 0°C, after LLPS occurs, the ACDAN fluorescence spectrum in the standard sample closely resembles the ACDAN fluorescence spectrum in the BSA sample measured at the same experimental condition. However, it also presents a minor additional component between 500 nm and 550 nm, which corresponds to the fluorescence signature of ACDAN in the PEG sample.

This indicates that, although some interactions between ACDAN and PEG are present, ACDAN molecules primarily experience a BSA-rich environment in the condensed phase. In particular, the preferential localization of ACDAN molecules in BSA-rich regions can be attributed to the strong interactions between ACDAN and BSA due to mainly hydrophobic effects.

This preference is also evident in the two-photon images, where ACDAN fluorescence is more intense in the condensed phase, which we have estimated to contain a BSA concentration approximately six times higher than that of the homogeneous phase. This suggests that ACDAN preferentially partitions into the denser phase due to its affinity for the protein-rich environment, likely driven by hydrophobic interactions.

To quantify the emission shift of ACDAN fluorescence spectra as a function of temperature, the Generalised Polarisation function (GP) was calculated as reported in the Materials and Methods section. GP was successfully used to monitor changes in DAN dyes[93,106–111]. The increase of GP values indicates a spectral blue-shift and therefore an increase of the phase ordering while its decrease denotes a spectral red-shift and thus the disordering of the phase. Figure 5b) shows that ACDAN GP changes as a function of temperature for the BSA sample (blue squares), standard sample (green circles), and the PEG sample (yellow triangles). As it is evident, GP measured in the BSA sample is positive at 35°C and increases almost linearly during the temperature ramp. Contrarily the GP measured in the PEG sample is negative at the same temperature and slightly decreases with decreasing temperature. The standard sample starts with a positive GP value, which

is intermediate between the initial GP values of the BSA sample and the PEG sample. This may suggest that in the homogeneous solution, ACDAN dye experiences an intermediate environment according to the ergodicity of the system. By lowering temperature this value increases and, importantly, it presents a biphasic behaviour. This is highlighted by the blue and the red dashed lines shown in Figure 5a). The blue dashed line corresponds to the slope of the initial growth of the GP measured in the standard sample and it is parallel to the GP data calculated in the BSA sample, suggesting that during the temperature ramp ACDAN is more sensitive to the BSA environment with respect to the PEG environment. This also denotes that the variation of GP values (and more in general of the fluorescence spectra) of the standard sample and the BSA sample are caused by the same thermal effects. A change of the slope is observed at about 21°C, which is the same temperature at which the trend inversion of the intensity of ACDAN fluorescence spectra is observable, as shown in Figure 4b). This temperature is also compatible with the transition temperature for this sample. At temperatures below 21°C the slope of the GP data increases as shown by the red dashed line.

Figure 5c) shows the spectral phasor analysis of the fluorescence spectra of the standard sample reported in the same colour code used in panel a. The coloured arrow denotes the progression along the temperature ramp from 35°C to 0°C and the green and the green and blue stars denote the data points corresponding to 21°C and 8°C, respectively. Spectral phasor analysis provides a graphical representation of the fluorescence data, reducing each spectrum to a point (phasor) in the phasor plot, which identifies the centroid and the width of the fluorescence band[48–51] . A reduction of the phase (the angle measured from the positive x-semiaxis) indicates a spectral blueshift and the decrease of the modulation (radius of the position of the data) the increase of the FWHM of the fluorescence spectrum[50,51].

BSA and PEG spectral phasor data, reported in Figure S5, undergo minor changes and present modification in the phase while no modulation changes are observed. Phase changes denote blue shift and the red shift occurring in the BSA and PEG samples respectively. These minor changes highlight what was already observed using GP analysis i.e. that these samples do not undergo phase transition. These shifts can only be associated with variations in the dipolar relaxation experienced by the ACDAN during the temperature ramp.

Conversely, the spectral phasors obtained for the standard sample, reported in Figure 5c, show a more complex S-shaped trend. A horizontal shift of the spectral phasors highlights a significant reduction in phase and modulation between 21°C and 8°C, marked in the plot by the green and blue stars. This horizontal trend can possibly be associated with the increased environmental heterogeneity experienced by the ACDAN molecule during the LLPS process.

To distinguish specific fluorescence features of the different phases formed following LLPS we analysed the two phases using fluorescence microscopy. A representative fluorescence image acquired by two-photon microscopy of the sample stained by ACDAN following the LLPS is reported in Figure 6a). The green spherical objects are the BSA coacervates, which present different sizes from few micrometres to 20 micrometres. The cyan and magenta circles indicate respectively the dense phase (i.e. the protein coacervates) and the diluted phase of the sample. The normalised ACDAN fluorescence spectra in the homogeneous phase (green squares), in the diluted phase (magenta circles), and in the coacervate phase (cyan triangles) are reported in Figure 6b). GP values calculated using the same wavelength of the previous analysis (450 nm and 560 nm), for the homogeneous, diluted, and concentrated phases are reported in Table 1. The sample used to acquire the image reported in Figure 6a), consists of 25 mg/ml BSA and 76 mg/ml PEG-4000. The PEG concentration was chosen to ensure LLPS occurs at room temperature (23°C) as shown in Figure 2. After LLPS takes place, ACDAN fluorescence signal mostly arises from protein condensates. The diluted phase presents a diffuse

fluorescence signal, in line with the fact that ACDAN is highly hydrophilic, but it is much lower than the fluorescence intensity detected within the coacervates.

This feature is in line with previous observations about the fluorescence spectra of ACDAN in standard sample resembling the one acquired for the BSA sample, suggesting that ACDAN preferentially partitions into the protein-rich environment (dense phase) due to its affinity with BSA molecules.

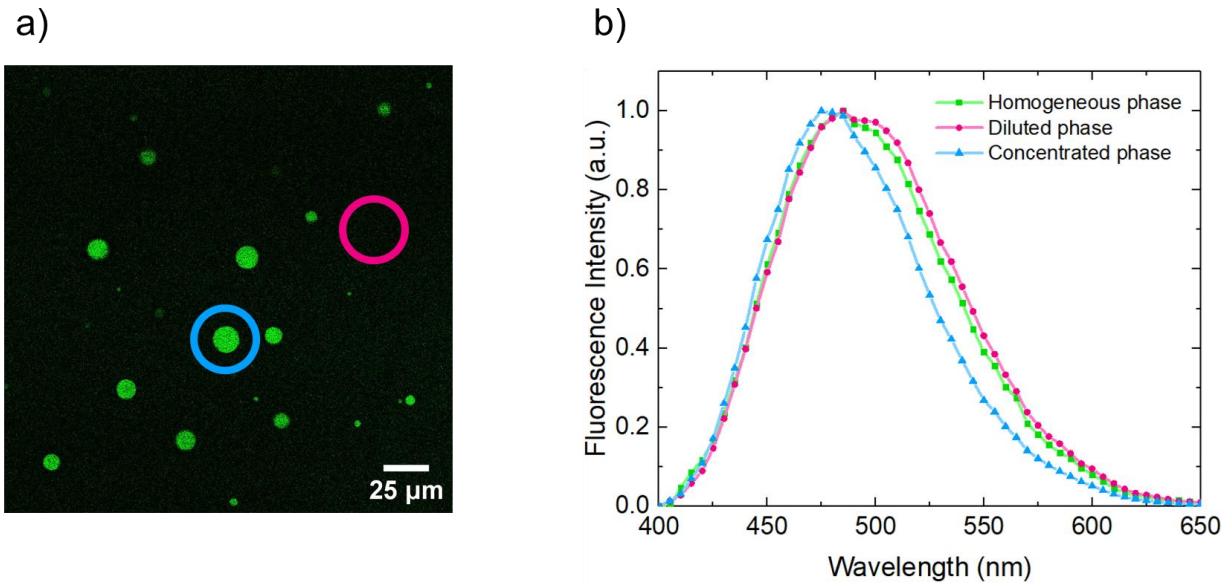

Figure 6*. a) A 1024×1024 pixels representative two-photon microscopy fluorescence image of the solution containing 76 mg/ml PEG-4000 at room temperature (23°C) stained with 30 µM ACDAN. Under these experimental conditions, the solution undergoes a LLPS. b) Normalised fluorescence spectra of homogeneous phase (green squares), diluted phase (magenta circles) and coacervate concentrated phase (cyan triangles), acquired by two-photon microscopy (λ_{exc} = 780 nm, bandwidth = 15 nm, step size = 5 nm). The homogeneous phase is the standard sample (68 mg/ml PEG) and the concentrated phase and diluted phase are obtained from a sample containing 76 mg/ml PEG and 25 mg/ml BSA. The concentrated phase spectrum and the diluted phase spectrum are respectively blue-shift and red-shifted with respect to the homogeneous phase.*

ACDAN fluorescence reported in Figure 6b) was excited at 780 nm and the fluorescence signal was acquired in the range between 400 nm and 650 nm. The fluorescence spectra were acquired at pixel resolution within the image, using a 15 nm bandwidth and 5 nm step size. These measurements were performed at room temperature (23°C), thus the PEG concentration was chosen consequently. The sample used for the homogeneous phase is the standard sample which has a transition temperature below room temperature, and the sample used for the diluted and concentrated phase contains 76 mg/ml PEG, which is already separated at room temperature as shown in Figure 6a). As already mentioned, it is reasonable to compare processes at different PEG concentrations, because the LLPS process is the same and what changes is the fraction of the dense phase that separates from the rest of the solution. The concentrated phase and the diluted phase were physically separated by centrifugation (10^4×g for 10 min at 20°C), since the protein coacervates which occur following LLPS are highly dynamic, and it could not be possible to perform long measurements as the one needed to acquire the fluorescence spectrum. However, the use of microscopy techniques was still necessary since the volume fraction of the dense phase is very small, being 20 µl for 1 ml of the total solution volume.

	Generalised Polarisation
Homogeneous Phase	0.339 ± 0.008
Diluted Phase	0.280 ± 0.014
Concentrated Phase	0.539 ± 0.005

Table 1: *Generalised Polarisation of ACDAN fluorescence spectra shown In Figure 5 calculated at 450 nm and 560 nm. The higher GP indicates a more ordered phase.*

To compare the microscopy results to the bulk reported above the ACDAN fluorescence spectra were corrected for instrumental response using the bulk spectra as a reference. The normalised fluorescence spectrum of the homogeneous phase sample is centred at 490 nm, in line with the data reported in Figure 4b. The spectrum is composed of two components; the blue component is centred at about 475 nm, and it is slightly more intense than the green component which is centred at about 500 nm. This results in a positive GP value GP = 0.339±0.008 in line with the GP value reported in Figure 4c. The concentrated phase spectrum has a higher blue component and a lower green, revealing a lower solvent dipolar relaxation and a higher molecular order. The GP value for the concentrated is 0.539 ± 0.005. On the contrary, the diluted phase spectrum is very similar to the homogeneous phase, indicating that the composition and the order degree of the diluted phase following the LLPS do not differ much from the ones of the homogeneous phase. However, it is possible to observe a slight but significant increase of the green component of the diluted phase with respect to the homogeneous phase. Following this, the calculated GP value for the diluted phase is 0.280 ± 0.014. This can be rationalised as many molecules (both protein and crowding agents) are segregated in the concentrated phase and therefore the molecular crowding and the excluded volume effects are decreased with respect to the initial homogeneous phase. This results in the increase of solvent dipolar relaxation and thus in the decrease of the overall molecular order of the phase.

To explore whether these modifications are detectable by the ACDAN fluorescence lifetime, FLIM measurements were performed on the concentrated phase and dilute phase. The concentrated phase and the diluted phase are obtained, as explained above, from a sample containing 76 mg/ml PEG and 25 mg/ml BSA, after centrifugation (10^4×g for 10 min at 20°C) to separate the two phases. ACDAN fluorescence lifetime has not been explored in any published paper, and only an abstract is available on this topic[112]. Therefore, the results will be interpreted and discussed on the basis of another DAN fluorescent probe, whose lifetime is much more studied, i.e. LAURDAN. LAURDAN is a hydrophobic dye which mainly partitions in lipid membranes and similarly to ACDAN, it is sensitive to the polarity of its environment and to the dipolar relaxation of water molecules around the LAURDAN molecule. FLIM analysis of LAURDAN fluorescence lifetime allows to disentangle these two properties, evaluating them separately, selecting the detection range properly. The blue channel allows the investigation of the polarity effects of the environment and the green channel allows the investigation of the dipolar relaxation of water molecules in the proximity of the fluorescent molecule.

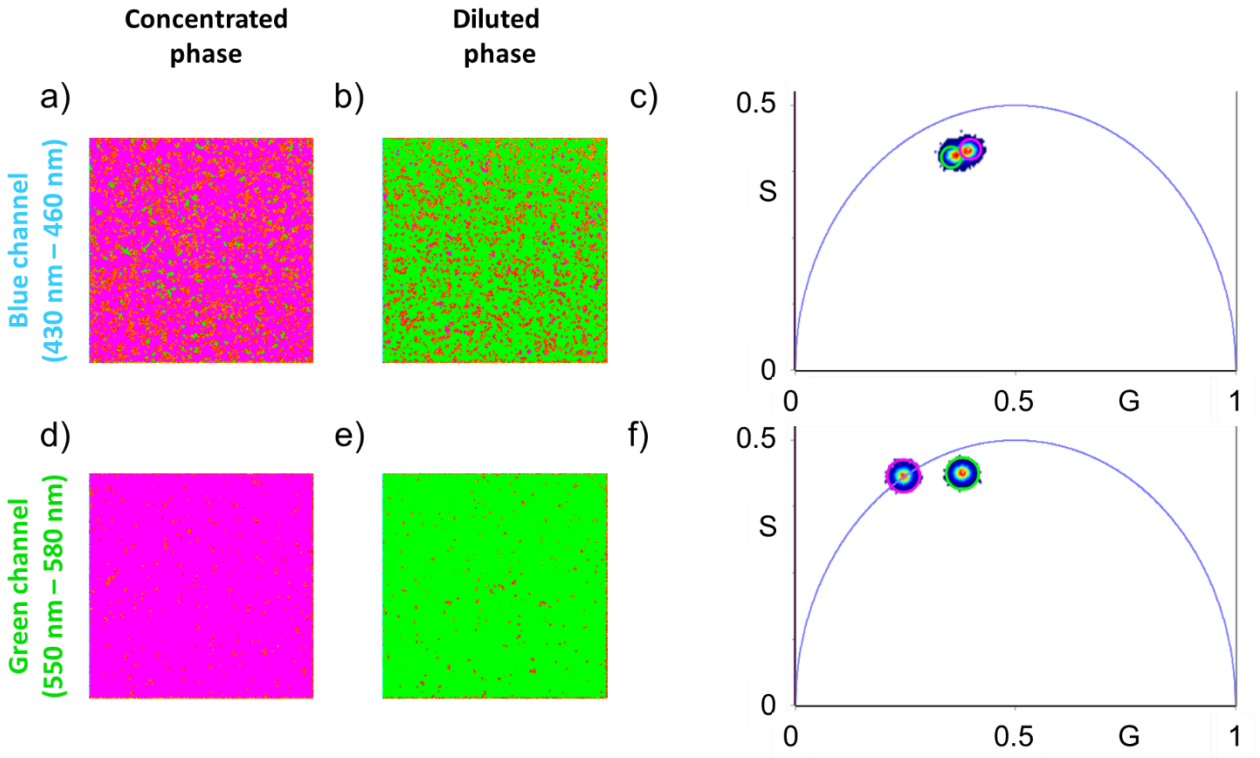

Figure 7. *FLIM data of ACDAN fluorescence analysed by means of the phasor approach: a-b) phasor maps of the a) concentrated phase and b) diluted phase acquired in the blue channel (430 nm – 460 nm) associated with the polarity of the micro-environment experienced by the ACDAN. c) Phasor plot shows two lifetime distributions that are selected by a magenta and green cursor. The phasor maps are coloured according to the colour of the cursors. FLIM data of ACDAN fluorescence analysed by means of the phasor approach: d-e) phasor maps of the d) concentrated phase and e) diluted phase acquired in the green channel (550 nm – 580 nm) associated to the solvent dipolar relaxation. f) Phasor plot shows two lifetime distributions that are selected by a magenta and green cursor. The phasor maps are coloured according to the colour of the cursors.*

In analogy with LAURDAN fluorescence, two acquisition ranges were selected to perform FLIM measurements. The blue channel was set as 430 nm – 460 nm and the green channel was set as 550 nm – 580 nm. FLIM data are analysed by means of the phasor approach, which provides a graphical representation of the data and does not require to impose an a priori model, which in contrary the fit analysis needs. Figure 7a-c) shows the phasor analysis of FLIM measurements on the diluted and concentrated phase in the blue channel. FLIM measurements of homogeneous samples are intended to provide a graphical representation of the data. As expected, the images do not show any structure over the diffraction images and only diffused ACDAN fluorescence is observed. The phasor plot in Figure 7c shows two lifetime distributions (clouds of points), selected by two coloured cursors. The green cursor was used to select the longer lifetime distribution and the magenta was used to select the shorter lifetime distribution. The phasor maps highlight that both the concentrated and diluted phase images are uniformly coloured respectively in magenta and in green. This denotes that each phase is homogeneous, as expected, and that ACDAN molecules experience slightly different polarity within the concentrated and diluted phases. In particular, the diluted phase presents a lower molecular crowding and therefore the water-protein ratio is higher. For these reasons, within the diluted phase (shorter lifetime) ACDAN is expected to experience a more polar environment, with respect to the concentrated phase (longer lifetime). Moreover, if a high contribution of ACDAN fluorescence derives from the ACDAN molecules which sense the hydration of BSA both outside and within the pockets, it is reasonable to assume that ACDAN molecules within the dense phase experience a less polar and more rigid environment. This is in line with the ACDAN spectral red-shift observed within the diluted phase.

Figure 7d-f) shows FLIM measurements analysed by phasor on the diluted phase and concentrated phase in the green channel. In Figure 7f) the phasor plot is reported, showing two well-distinct lifetime distributions. In line with the analysis reported above, the two lifetime distributions are selected by two cursors: the shorter lifetime distribution is selected by a magenta cursor and the longer lifetime distribution is selected by a green cursor. Looking at the phasor maps it is evident that the lifetime distribution selected by the magenta cursor is associated with the concentrated phase (panel d) and the lifetime distribution selected by the green one is associated with the diluted phase (panel e). Also in this case, the phasor maps are homogeneously coloured by single colours, denoting that the dipolar relaxation of water is quite different in the two phases. The water dipolar relaxation within the concentrated phase is higher because the environment is more crowded. Moreover, since fewer water molecules are presented with respect to the BSA molecules, as discussed above, BSA molecules are more dehydrated and the overall environment more rigid. This results in an increase of ACDAN fluorescence lifetime. The opposite, the diluted phase which presents a shorter ACDAN fluorescence lifetime, shows a higher dipolar relaxation, in line with the data reported in Figure 6).

4. Conclusion

Over the past decades, LLPS has emerged as a compelling field of study. Although there have been notable breakthroughs, our comprehension of LLPS mechanisms and internal physico-chemistry remains in its early stages. In this work, the LLPS process of a BSA and PEG solution was investigated. PEG was used as a crowding agent and the LLPS was induced by thermal effects. The main aim of the study is to explore the role of water in LLPS processes and how its ordering is modified during and by the transition. PEG, a widely used polymer, is known for its ability to induce phase separation through volume exclusion effects, which effectively increase the local concentration of proteins by reducing the available volume in the solution. PEG concentration was systematically varied, and this results in the observation that higher concentrations significantly promoted phase separation, in line with the literature. This was demonstrated by an increase in scattering intensity at lower temperatures, suggesting the formation of BSA-rich coacervates and subsequent phase separation. To gain information on BSA-PEG phase separation, the impact of two ordering and disordering co-solutes was explored. By monitoring the scattering intensity it was also possible to explore the effects of non-ionic kosmotropic compounds, such as glycerol, and non-ionic chaotropic compounds, such as ethanol, on LLPS. The reported results showed that ethanol promotes the LLPS increasing the transition temperature, while glycerol suppresses the process, acting as a stabilising agent. This is probably due to the effects of the two compounds on the hydration shell of BSA, but effects due to viscosity and direct interactions with the protein molecules cannot be excluded. Finally, the effect of LLPS on water ordering was examined by using the fluorescent dye 6-acetyl-2-dimethylamino naphthalene (ACDAN). ACDAN fluorescence properties allowed us to gain insights into the interior physical-chemistry changes occurring during phase separation. ACDAN was observed to be sensitive to the LLPS and it experiences different environments within the concentrated phase (BSA coacervates) and the diluted phase. Data also suggests that ACDAN interacts with BSA molecules and therefore it is more sensitive to BSA-bound water. By monitoring the fluorescence spectra of ACDAN in solutions of BSA and PEG, we observed significant variations between the condensed and diluted phases. Moreover, the fluorescence lifetime of ACDAN was analysed by means of the phasor approach. Thus, it was possible to disentangle the two factors which affect its fluorescence, being polarity and solvent dipolar relaxation. Overall, the diluted phase was observed to be more polar and with a higher dipolar relaxation with respect to the concentrated phase. This comprehensive

investigation contributes to a deeper understanding of the molecular mechanisms underlying LLPS in protein solutions, by elucidating the roles of crowding agents and water dynamics.

5. References

1. Sun, Y. *et al.* Phase-separating peptides for direct cytosolic delivery and redox-activated release of macromolecular therapeutics. *Nat Chem* **14**, (2022).

2. Saini, B. & Mukherjee, T. K. Biomolecular Condensates Regulate Enzymatic Activity under a Crowded Milieu: Synchronization of Liquid-Liquid Phase Separation and Enzymatic Transformation. *Journal of Physical Chemistry B* **127**, (2023).

3. Gong, J., Tsumura, N., Sato, Y. & Takinoue, M. Computational DNA Droplets Recognizing miRNA Sequence Inputs Based on Liquid–Liquid Phase Separation. *Adv Funct Mater* **32**, (2022).

4. Linsenmeier, M. *et al.* The interface of condensates of the hnRNPA1 low-complexity domain promotes formation of amyloid fibrils. *Nat Chem* **15**, (2023).

5. Mitrea, D. M., Mittasch, M., Gomes, B. F., Klein, I. A. & Murcko, M. A. Modulating biomolecular condensates: a novel approach to drug discovery. *Nat Rev Drug Discov* **21**, (2022).

6. Xu, Z., Wang, W., Cao, Y. & Xue, B. Liquid-liquid phase separation: Fundamental physical principles, biological implications, and applications in supramolecular materials engineering. *Supramolecular Materials* vol. 2 Preprint at https://doi.org/10.1016/j.supmat.2023.100049 (2023).

7. Gomes, E. & Shorter, J. The molecular language of membraneless organelles. *Journal of Biological Chemistry* vol. 294 7115–7127 Preprint at https://doi.org/10.1074/jbc.TM118.001192 (2019).

8. Hyman, A. A., Weber, C. A. & Jülicher, F. Liquid-liquid phase separation in biology. *Annual review of cell and developmental biology* vol. 30 39–58 Preprint at https://doi.org/10.1146/annurev-cellbio-100913-013325 (2014).

9. Wang, B. *et al.* Liquid–liquid phase separation in human health and diseases. *Signal Transduction and Targeted Therapy* vol. 6 Preprint at https://doi.org/10.1038/s41392-021-00678-1 (2021).

10. Banani, S. F., Lee, H. O., Hyman, A. A. & Rosen, M. K. Biomolecular condensates: Organizers of cellular biochemistry. *Nature Reviews Molecular Cell Biology* vol. 18 285–298 Preprint at https://doi.org/10.1038/nrm.2017.7 (2017).

11. Courchaine, E. M., Lu, A. & Neugebauer, K. M. Droplet organelles? *EMBO J* **35**, 1603–1612 (2016).

12. Alberti, S., Gladfelter, A. & Mittag, T. Considerations and Challenges in Studying Liquid-Liquid Phase Separation and Biomolecular Condensates. *Cell* vol. 176 419–434 Preprint at https://doi.org/10.1016/j.cell.2018.12.035 (2019).

13. Pezzotti, S., König, B., Ramos, S., Schwaab, G. & Havenith, M. Liquid-Liquid Phase Separation? Ask the Water! *Journal of Physical Chemistry Letters* **14**, (2023).

14. Ribeiro, S. S., Samanta, N., Ebbinghaus, S. & Marcos, J. C. The synergic effect of water and biomolecules in intracellular phase separation. *Nature Reviews Chemistry* vol. 3 Preprint at https://doi.org/10.1038/s41570-019-0120-4 (2019).

15. Yu, I. & Nagaoka, M. Slowdown of water diffusion around protein in aqueous solution with ectoine. *Chem Phys Lett* **388**, (2004).

16. Russo, D. The impact of kosmotropes and chaotropes on bulk and hydration shell water dynamics in a model peptide solution. *Chem Phys* **345**, (2008).

17. Marcus, Y. Effect of ions on the structure of water: Structure making and breaking. *Chemical Reviews* vol. 109 Preprint at https://doi.org/10.1021/cr8003828 (2009).

18. Chaaban, H., Vallooran, J. J., Van De Weert, M. & Foderà, V. Ion-Mediated Morphological Diversity in Protein Amyloid Systems. *Journal of Physical Chemistry Letters* **13**, (2022).

19. Poudyal, M. *et al.* Intermolecular interactions underlie protein/peptide phase separation irrespective of sequence and structure at crowded milieu. *Nat Commun* **14**, (2023).

20. Krainer, G. *et al.* Reentrant liquid condensate phase of proteins is stabilized by hydrophobic and non-ionic interactions. *Nat Commun* **12**, (2021).

21. De Luca, G., Sancataldo, G., Militello, B. & Vetri, V. Surface-catalyzed liquid–liquid phase separation and amyloid-like assembly in microscale compartments. *J Colloid Interface Sci* **676**, 569–581 (2024).

22. Park, S. *et al.* Dehydration entropy drives liquid-liquid phase separation by molecular crowding. *Commun Chem* **3**, (2020).

23. Zaslavsky, B. Y. & Uversky, V. N. In Aqua Veritas: The Indispensable yet Mostly Ignored Role of Water in Phase Separation and Membrane-less Organelles. *Biochemistry* vol. 57 Preprint at https://doi.org/10.1021/acs.biochem.7b01215 (2018).

24. Peyrin, E., Guillaume, Y. C. & Guinchard, C. Characterization of solute binding at human serum albumin site II and its geometry using a biochromatographic approach. *Biophys J* **77**, (1999).

25. Anselmo, S. *et al.* Lead(II) ions adsorption onto amyloid particulates: An in depth study. *J Colloid Interface Sci* **610**, (2022).

26. Ramos, S. *et al.* Hydration makes a difference! How to tune protein complexes between liquid-liquid and liquid-solid phase separation. *Physical Chemistry Chemical Physics* **25**, (2023).

27. Anselmo, S. *et al.* Sustainable soy protein microsponges for efficient removal of lead (II) from aqueous environments. *Int J Biol Macromol* **239**, (2023).

28. Rego, N. B., Xi, E. & Patel, A. J. Identifying hydrophobic protein patches to inform protein interaction interfaces. *Proc Natl Acad Sci U S A* **118**, (2021).

29. Adams, E. M. *et al.* Local Mutations Can Serve as a Game Changer for Global Protein Solvent Interaction. *JACS Au* **1**, (2021).

30. Wang, Y., Lomakin, A., Kanai, S., Alex, R. & Benedek, G. B. Liquid-Liquid Phase Separation in Oligomeric Peptide Solutions. *Langmuir* **33**, (2017).

31. Moron, M. *et al.* Gelation Dynamics upon Pressure-Induced Liquid-Liquid Phase Separation in a Water-Lysozyme Solution. *Journal of Physical Chemistry B* **126**, 4160–4167 (2022).

32. Da Vela, S. *et al.* Kinetics of liquid-liquid phase separation in protein solutions exhibiting LCST phase behavior studied by time-resolved USAXS and VSANS. *Soft Matter* **12**, 9334–9341 (2016).

33. Van Lindt, J. *et al.* A generic approach to study the kinetics of liquid–liquid phase separation under near-native conditions. *Commun Biol* **4**, (2021).

34. Džudžević Čančar, H., Belak Vivod, M., Vlachy, V. & Lukšič, M. Phase stability of aqueous mixtures of bovine serum albumin with low molecular mass salts in presence of polyethylene glycol. *J Mol Liq* **349**, (2022).

35. Li, R., Wu, Z., Wangb, Y., Ding, L. & Wang, Y. Role of pH-induced structural change in protein aggregation in foam fractionation of bovine serum albumin. *Biotechnology Reports* **9**, (2016).

36. Salgin, S., Salgin, U. & Bahadir, S. Zeta potentials and isoelectric points of biomolecules: The effects of ion types and ionic strengths. *Int J Electrochem Sci* **7**, (2012).

37. Matsarskaia, O. *et al.* Phase-Separation Kinetics in Protein-Salt Mixtures with Compositionally Tuned Interactions. *Journal of Physical Chemistry B* **123**, (2019).

38. Maier, R., Fries, M. R., Buchholz, C., Zhang, F. & Schreiber, F. Human versus Bovine Serum Albumin: A Subtle Difference in Hydrophobicity Leads to Large Differences in Bulk and Interface Behavior. *Cryst Growth Des* **21**, (2021).

39. Testa, A. *et al.* Sustained enzymatic activity and flow in crowded protein droplets. *Nat Commun* **12**, (2021).

40. Bullier-Marchandin, E. *et al.* Investigation of the Formation and Aging of Albumin-Based Condensates. *ACS Applied Engineering Materials* **1**, (2023).

41. Majorek, K. A. *et al.* Structural and immunologic characterization of bovine, horse, and rabbit serum albumins. *Mol Immunol* **52**, (2012).

42. M, H., Azzazy, E. & Christenson, R. H. All About Albumin: Biochemistry, Genetics, and Medical Applications. Theodore Peters, Jr. San Diego, CA: Academic Press, 1996, 432 pp, $85.00. ISBN 0-12-552110-3. *Clin Chem* **43**, (1997).

43. Weber, G. & Farris, F. J. Synthesis and Spectral Properties of a Hydrophobic Fluorescent Probe: 6-Propionyl-2-(dimethylamino)naphthalene. *Biochemistry* **18**, (1979).

44. Otaiza-González, S. *et al.* The innards of the cell: studies of water dipolar relaxation using the ACDAN fluorescent probe. *Methods Appl Fluoresc* **10**, (2022).

45. Vorontsova, I. *et al.* In vivo macromolecular crowding is differentially modulated by aquaporin 0 in zebrafish lens: Insights from a nanoenvironment sensor and spectral imaging. *Sci Adv* **8**, (2022).

46. Mangiarotti, A. *et al.* Biomolecular condensates modulate membrane lipid packing and hydration. *Nat Commun* **14**, (2023).

47. Parasassi, T., De Stasio, G., Ravagnan, G., Rusch, R. M. & Gratton, E. Quantitation of lipid phases in phospholipid vesicles by the generalized polarization of Laurdan fluorescence. *Biophys J* **60**, (1991).

48. Fereidouni, F., Bader, A. N. & Gerritsen, H. C. Spectral phasor analysis allows rapid and reliable unmixing of fluorescence microscopy spectral images. *Opt Express* **20**, (2012).

49. Fereidouni, F., Bader, A. N., Colonna, A. & Gerritsen, H. C. Phasor analysis of multiphoton spectral images distinguishes autofluorescence components of in vivo human skin. *J Biophotonics* **7**, (2014).

50. Malacrida, L., Gratton, E. & Jameson, D. M. Model-free methods to study membrane environmental probes: A comparison of the spectral phasor and generalized polarization approaches. *Methods Appl Fluoresc* **3**, (2015).

51. Malacrida, L. & Gratton, E. LAURDAN fluorescence and phasor plots reveal the effects of a H2O2 bolus in NIH-3T3 fibroblast membranes dynamics and hydration. *Free Radic Biol Med* **128**, (2018).

52. Digman, M. A., Caiolfa, V. R., Zamai, M. & Gratton, E. The phasor approach to fluorescence lifetime imaging analysis. *Biophys J* **94**, (2008).

53. Torrado Belen, Pannunzio Bruno, Malacrida Leonel & Digman Michelle A. Fluorescence lifetime imaging microscopy. *Nature Reviews Methods Primers* **80**, (2024).

54. van Zanten, C., Melnikau, D. & Ryder, A. G. Effects of Viscosity and Refractive Index on the Emission and Diffusion Properties of Alexa Fluor 405 Using Fluorescence Correlation and Lifetime Spectroscopies. *J Fluoresc* **31**, (2021).

55. Magde, D., Rojas, G. E. & Seybold, P. G. Solvent dependence of the fluorescence lifetimes of xanthene dyes. *Photochem Photobiol* **70**, (1999).

56. Wang, Y. & Annunziata, O. Comparison between Protein-polyethylene Glycol (PEG) interactions and the effect of PEG on protein-protein interactions using the liquid-liquid phase transition. *Journal of Physical Chemistry B* **111**, (2007).

57. Annunziata, O. *et al.* Effect of polyethylene glycol on the liquid-liquid phase transition in aqueous protein solutions. *Proc Natl Acad Sci U S A* **99**, (2002).

58. Alfano, C. *et al.* Molecular Crowding: The History and Development of a Scientific Paradigm. *Chem Rev* **0**, (2024).

59. Nguemaha, V., Qin, S. & Zhou, H. X. Transfer free energies of test proteins into crowded protein solutions have simple dependence on crowder concentration. *Front Mol Biosci* **6**, (2019).

60. Kaur, T. *et al.* Molecular crowding tunes material states of ribonucleoprotein condensates. *Biomolecules* **9**, (2019).

61. Julius, K. *et al.* Impact of Macromolecular Crowding and Compression on Protein-Protein Interactions and Liquid-Liquid Phase Separation Phenomena. *Macromolecules* **52**, (2019).

62. Song, J. *et al.* Freezing-mediated formation of supraproteins using depletion forces. *J Colloid Interface Sci* **665**, (2024).

63. Kulkarni, A. M., Chatterjee, A. P., Schweizer, K. S. & Zukoski, C. F. Effects of polyethylene glycol on protein interactions. *Journal of Chemical Physics* **113**, (2000).

64. Sakuta, H. *et al.* Self-Emergent Protocells Generated in an Aqueous Solution with Binary Macromolecules through Liquid-Liquid Phase Separation. *ChemBioChem* **21**, (2020).

65. André, A. A. M. & Spruijt, E. Liquid–liquid phase separation in crowded environments. *Int J Mol Sci* **21**, (2020).

66. Waizumi, T. *et al.* Polymerization/depolymerization of actin cooperates with the morphology and stability of cell-sized droplets generated in a polymer solution under a depletion effect. *Journal of Chemical Physics* **155**, (2021).

67. Najafi, S. *et al.* Liquid–liquid phase separation of Tau by self and complex coacervation. *Protein Science* **30**, (2021).

68. Bhat, R. & Timasheff, S. N. Steric exclusion is the principal source of the preferential hydration of proteins in the presence of polyethylene glycols. *Protein Science* **1**, (1992).

69. Shulgin, I. L. & Ruckenstein, E. Preferential hydration and solubility of proteins in aqueous solutions of polyethylene glycol. *Biophys Chem* **120**, (2006).

70. Stewart, C. J., Olgenblum, G. I., Propst, A., Harries, D. & Pielak, G. J. Resolving the enthalpy of protein stabilization by macromolecular crowding. *Protein Science* **32**, (2023).

71. Hallsworth, J. E., Prior, B. A., Nomura, Y., Iwahara, M. & Timmis, K. N. Compatible Solutes Protect against Chaotrope (Ethanol)-Induced, Nonosmotic Water Stress. *Appl Environ Microbiol* **69**, (2003).

72. Abou-Saleh, R. H. *et al.* Molecular Effects of Glycerol on Lipid Monolayers at the Gas-Liquid Interface: Impact on Microbubble Physical and Mechanical Properties. *Langmuir* **35**, (2019).

73. Tange, H. *et al.* Liquid liquid phase separation of full-length prion protein initiates conformational conversion in vitro. *Journal of Biological Chemistry* **296**, (2021).

74. Vetri, V. *et al.* Ethanol Controls the Self-Assembly and Mesoscopic Properties of Human Insulin Amyloid Spherulites. *Journal of Physical Chemistry B* **122**, (2018).

75. Chong, Y., Kleinhammes, A., Tang, P., Xu, Y. & Wu, Y. Dominant alcohol-protein interaction via hydration-enabled enthalpy-driven binding mechanism. *Journal of Physical Chemistry B* **119**, (2015).

76. Yoshikawa, H., Hirano, A., Arakawa, T. & Shiraki, K. Mechanistic insights into protein precipitation by alcohol. *Int J Biol Macromol* **50**, (2012).

77. Juárez, J. *et al.* Hydration effects on the fibrillation process of a globular protein: The case of human serum albumin. *Soft Matter* **8**, (2012).

78. Zhang, H. *et al.* Research on the secondary structure and hydration water around human serum albumin induced by ethanol with infrared and near-infrared spectroscopy. *J Mol Struct* **1275**, (2023).

79. Bäcklund, F. G. & Solin, N. Tuning the aqueous self-assembly process of insulin by a hydrophobic additive. *RSC Adv* **5**, (2015).

80. Koizumi, M., Hirai, H., Onai, T., Inoue, K. & Hirai, M. Collapse of the hydration shell of a protein prior to thermal unfolding. in *Journal of Applied Crystallography* vol. 40 (2007).

81. Dzwolak, W. *et al.* Ethanol-perturbed amyloidogenic self-assembly of insulin: Looking for origins of amyloid strains. *Biochemistry* **44**, (2005).

82. Ghosh, R., Samajdar, R. N., Bhattacharyya, A. J. & Bagchi, B. Composition dependent multiple structural transformations of myoglobin in aqueous ethanol solution: A combined experimental and theoretical study. *Journal of Chemical Physics* **143**, (2015).

83. Chattoraj, S., Mandal, A. K. & Bhattacharyya, K. Effect of ethanol-water mixture on the structure and dynamics of lysozyme: A fluorescence correlation spectroscopy study. *Journal of Chemical Physics* **140**, (2014).

84. Liu, R. *et al.* Toxic effects of ethanol on bovine serum albumin. *J Biochem Mol Toxicol* **24**, (2010).

85. Javid, N., Vogtt, K., Krywka, C., Tolan, M. & Winter, R. Protein-protein interactions in complex cosolvent solutions. *ChemPhysChem* **8**, (2007).

86. Koynova, R., Brankov, J. & Tenchov, B. Modulation of lipid phase behavior by kosmotropic and chaotropic solutes. Experiment and thermodynamic theory. *European Biophysics Journal* **25**, (1997).

87. Charkhesht, A. *et al.* Insights into Hydration Dynamics and Cooperative Interactions in Glycerol-Water Mixtures by Terahertz Dielectric Spectroscopy. *Journal of Physical Chemistry B* **123**, (2019).

88. Timasheff, S. N. Protein-solvent preferential interactions, protein hydration, and the modulation of biochemical reactions by solvent components. *Proc Natl Acad Sci U S A* **99**, (2002).

89. Segur, J. B. & Oderstar, H. E. Viscosity of Glycerol and Its Aqueous Solutions. *Ind Eng Chem* **43**, (1951).

90. González-Tello, P., Camacho, F. & Blázquez, G. Density and Viscosity of Concentrated Aqueous Solutions of Polyethylene Glycol. *J Chem Eng Data* **39**, (1994).

91. Hirai, M. *et al.* Direct Evidence for the Effect of Glycerol on Protein Hydration and Thermal Structural Transition. *Biophys J* **115**, (2018).

92. Begarani, F. *et al.* Capturing Metabolism-Dependent Solvent Dynamics in the Lumen of a Trafficking Lysosome. *ACS Nano* **13**, (2019).

93. Thoke, H. S. *et al.* Tight coupling of metabolic oscillations and intracellular water dynamics in Saccharomyces cerevisiae. *PLoS One* **10**, (2015).

94. Ambroggio, E. E., Navarro, G. S. C., Socas, L. B. P., Bagatolli, L. A. & Gamarnik, A. V. Dengue and Zika virus capsid proteins bind to membranes and self-assemble into liquid droplets with nucleic acids. *Journal of Biological Chemistry* **297**, (2021).

95. Zeng, J. & Chong, P. L. Effect of ethanol-induced lipid interdigitation on the membrane solubility of Prodan, Acdan, and Laurdan. *Biophys J* **68**, (1995).

96. De Luca, G., Ferrara, V., Pignataro, B., Vetri, V. & Sancataldo, G. A Fluorescent Perspective on Water Structuring: ACDAN in Salt Solutions and Hydrogels. *Biophysica* **4**, 619–633 (2024).

97. Gunther, G., Malacrida, L., Jameson, D. M., Gratton, E. & Sánchez, S. A. LAURDAN since Weber: The Quest for Visualizing Membrane Heterogeneity. *Acc Chem Res* **54**, (2021).

98. Oliva, R., Banerjee, S., Cinar, H., Ehrt, C. & Winter, R. Alteration of Protein Binding Affinities by Aqueous Two-Phase Systems Revealed by Pressure Perturbation. *Sci Rep* **10**, (2020).

99. Shahid, M. & Chawla, H. M. Dansylated adenine as a molecular probe for exploring hydrophobic pocket of bovine serum albumin (BSA) and its utility for mercury ion recognition. *J Lumin* **188**, (2017).

100. Moriyama, Y., Ohta, D., Hachiya, K., Mitsui, Y. & Takeda, K. Fluorescence behavior of tryptophan residues of bovine and human serum albumins in ionic surfactant solutions: A comparative study of the two and one tryptophan(s) of bovine and human albumins. *J Protein Chem* **15**, (1996).

101. Vetri, V., Librizzi, F., Leone, M. & Militello, V. Thermal aggregation of bovine serum albumin at different pH: Comparison with human serum albumin. in *European Biophysics Journal* vol. 36 (2007).

102. Cattoni, D. I., Kaufman, S. B. & Flecha, F. L. G. Kinetics and thermodynamics of the interaction of 1-anilino-naphthalene-8-sulfonate with proteins. *Biochim Biophys Acta Proteins Proteom* **1794**, (2009).

103. Ota, C., Tanaka, S. I. & Takano, K. Revisiting the rate-limiting step of the ans–protein binding at the protein surface and inside the hydrophobic cavity. *Molecules* **26**, (2021).

104. Militello, V., Vetri, V. & Leone, M. Conformational changes involved in thermal aggregation processes of bovine serum albumin. *Biophys Chem* **105**, (2003).

105. Lakowicz, J. R. *Principles of Fluorescence Spectroscopy*. *Principles of Fluorescence Spectroscopy* (2006). doi:10.1007/978-0-387-46312-4.

106. Thoke, H. S., Thorsteinsson, S., Stock, R. P., Bagatolli, L. A. & Olsen, L. F. The dynamics of intracellular water constrains glycolytic oscillations in Saccharomyces cerevisiae. *Sci Rep* **7**, (2017).

107. Van Maarschalkerweerd, A., Vetri, V. & Vestergaard, B. Cholesterol facilitates interactions between α-synuclein oligomers and charge-neutral membranes. *FEBS Lett* **589**, (2015).

108. Golfetto, O., Hinde, E. & Gratton, E. Laurdan fluorescence lifetime discriminates cholesterol content from changes in fluidity in living cell membranes. *Biophys J* **104**, (2013).

109. Anselmo, S., Sancataldo, G., Mørck Nielsen, H., Foderà, V. & Vetri, V. Peptide-Membrane Interactions Monitored by Fluorescence Lifetime Imaging: A Study Case of Transportan 10. *Langmuir* **37**, (2021).

110. Soto-Arriaza, M. A., Sotomayor, C. P. & Lissi, E. A. Relationship between lipid peroxidation and rigidity in L-α-phosphatidylcholine-DPPC vesicles. *J Colloid Interface Sci* **323**, (2008).

111. Anselmo, S., Sancataldo, G., Baiamonte, C., Pizzolanti, G. & Vetri, V. Transportan 10 Induces Perturbation and Pores Formation in Giant Plasma Membrane Vesicles Derived from Cancer Liver Cells. *Biomolecules* **13**, (2023).

112. Palomba, F., Scipioni, L., Gratton, E. & Digman, M. A. Water Dynamics of a Model Protein Phase Separation via Fluorescence Lifetime and Spectral Analysis of ACDAN. *Biophys J* **118**, (2020).

CRediT authorship contribution statement

Declaration of Competing Interest

The authors declare that they have no competing interests.

Fundings

This work received funding from MUR - PRIN PNRR - LLPS (Liquid-Liquid Phase Separation Dynamics in Biomimetic Compartments), and FFR Unipa 2023 and FFR Unipa 2024.

Data availability

The datasets used and/or analysed during the current study are available from the corresponding author upon reasonable request.